Scaling Behavior of the Elastic Modulus in Colloidal Networks of Fat Crystals

Tarek S. Awad, Michael A. Rogers, and Alejandro G. Marangoni*

Department of Food Science, University of Guelph, Guelph, ON N1G2W1, Canada

Received: August 4, 2003; In Final Form: October 23, 2003

The scaling relationship between the shear elastic modulus and the solid fat content (SFC) was determined for anhydrous milk fat (AMF), palm oil (PO), and cocoa butter (CB). The fats were diluted with canola oil to achieve specific SFCs and crystallized at 5 °C for 24 h. SFC decreased linearly by increasing the canola oil mass fraction as determined by pulsed NMR. Log−log plots of the shear storage modulus (G') versus the solids' volume fraction (Φ = SFC/100) of the diluted fats were used to determine the fractal dimension (D) of the networks. Three different linear regions were identified for the range of dilutions studied. The scaling relationship of the stress at the limit of linearity (σ_o) to Φ indicated that the fats were in the weak-link rheological regime in all three regions. These results suggested that three different types of weak-link rheological regimes could be present in the same material depending on the SFC. Polarized light microscopy showed that varying the solid fat content (SFC) modified the microstructure of these fats. In general, at low SFCs, large crystal clusters were observed, while at high SFCs, only a fine crystal mass was detected. Crystallite morphology and size distribution was also affected by dilution. The onset of crystallization temperature (T_c) and the peak melting temperature decreased with decreasing SFC in the three fats; however, plots of T_c versus SFC demonstrated the existence of distinct linear regions that were similar to those identified in the rheological data. Moreover, Hildebrand plots also demonstrated the existence of distinct linear regions, of characteristic solution behavior, which agreed closely with crystallization and rheological results. We propose that, upon dilution, changes in crystal phase behavior lead to changes in the crystallization kinetics of the fats. This in turn translated into alterations in the microstructure of the fat, which ultimately affected its mechanical properties.

Introduction

Fats are the main structural components in many food products such as margarine, chocolate, butter, and spreads. The sensory characteristics of fat-structured materials such as spreadability, hardness, and mouth feel are highly dependent on the structure of the underlying fat crystal network, which controls its macroscopic rheological properties.[1−5] This fat crystal network is built by the interaction of polycrystalline fat particles, which provides firmness or solidlike behavior to the plastic fats.[1−5] The amount, geometry, and spatial distribution of solid fat crystals as well as their interactions at different levels within the network all affect the rheological properties of fats and fat-structured food products.

Structural analogies between fat crystal networks and colloidal gels have been drawn since 1961.[6,7] Vreeker et al.[8] first proposed that a network of tristearin crystals in paraffin oil resembled a colloidal gel that could be analyzed using fractal scaling theories. Our group has developed this concept further by relating the different structural levels in a fat crystal network to macroscopic elastic properties.[9−11] Further studies[12−14] have shown that consideration of the mesoscale level of structure is important in modeling the mechanical properties of fat crystal networks.

The scaling behavior of the elastic modulus with solids' volume fraction in flocculated colloidal aggregates has been studied extensively[15−22] and a theory was developed to relate the elastic properties of colloidal gels to their structure.[16] Subsequently, Shih et al.[18] proposed the existence of two rheological regimes, namely, the strong-link regime at low solids' volume fractions and the weak-link regime at high solids' volume fractions. Recently, a transition regime was proposed by Wu and Morbidelli.[22] In these studies, the fractal concept was used to characterize the spatial distribution of the gel network mass. The fractal dimension (D), which defines the cluster size, has been evaluated by light scattering and rheology techniques[8,17−23] and more recently by microscopy.[24−26] Rheology is the most common technique for the quantification of microstructure in fat crystal networks by utilizing the relationship of the shear storage modulus (G') to the volume fraction of network solid mass (Φ) via the mass fractal dimension (D) of the network. In previous work from our group, we considered that fat crystal networks, at relatively high solid fat contents, were in the weak-link rheological regime.[9,10] This is because crystal clusters are relatively hard structures, not likely to yield at small deformations and, instead, the links between theses hard spheres would yield. However, conclusive evidence for the existence of these rheological regimes in fat systems has not been provided yet.

In this work, we demonstrate the scaling behavior of the elastic modulus with solid fat content (SFC) in fats and examine the occurrence of the two common rheological link regimes (i.e., weak and strong). For this purpose, the rheological properties of three common fats were determined at different SFCs. For each fat, the existence of a particular rheological link regime was confirmed, as in colloidal gels, by studying the behavior of the stress at the limit of linearity at different SFCs. In addition, the feasibility of using the stress at the limit of linearity to obtain structural information about the fat crystal network and to

* Corresponding author. E-mail: amarango@uoguelph.ca.

10.1021/jp036285u CCC: $27.50
Published on Web 11/27/2003

determine the mass fractal dimension was also investigated. We also monitored changes in the microstructure of the fats upon variation of SFC to determine whether there is a relationship between mechanical properties, crystallization behavior, and network structure.

Theory

Vreeker et al.[8] showed that the storage modulus (G') of an aggregated fat crystal network changed with particle concentration (Φ) according to a power law, similarly to flocculated colloidal gels. Subsequently, Marangoni and Rousseau[9] applied the theory of Shih et al.[18] to fats at high SFC, assuming the weak-link regime. According to the scaling theory of Shih et al., the scaling behavior of the elastic properties of colloidal gels can belong to either of two regimes. These regimes are dependent on the strength of the links between the clusters (microstructures in the fat crystal network) of a colloidal gel relative to the strength of the clusters themselves.

Strong-Link Regime. In the strong link regime, the individual flocs or clusters of colloidal gels grow large, so that each cluster acts as a weak spring. As a result, the elastic constant of the system as a function of particle concentration is dominated by the elastic constant of the flocs and not by the elastic constant between the flocs (interfloc links). The expression for the strong-link regime, as proposed by Shih et al.[18] is

$$K \sim \Phi^{[(d+x)/(d-D)]} \tag{1}$$

where K [N/m] is the macroscopic elastic constant, d is the Euclidean dimension, x is the chemical length exponent or backbone fractal dimension and is usually assumed to have a value between 1 and 1.3, and D is the fractal dimension of the flocs. Therefore, the elastic modulus increases with the particle volume fraction in a power law manner with an exponent $[(d + x)/ (d - D)]$.

Weak-Link Regime. In the weak-link regime, the interfloc links are weak compared to the flocs and can be considered as small rigid springs. The elastic constant of the system, thus, is dominated by the elastic constant of interfloc links, which is weaker than that of the flocs. This behavior is observed at high particle concentrations. The elastic constant (K) of a system in the weak-link regime can be expressed as

$$K \sim \Phi^{(d-2)/(d-D)} \tag{2}$$

Therefore, the elastic modulus increases with the particle volume fraction in a power law manner with an exponent $[(d - 2)/ (d - D)]$.

Thus, the relationship between the elastic constant K and solids' volume fraction Φ yields a straight line with slope equal to $(3 + x)/(3 - D)$ in the strong-link regime, or $1/(3 - D)$ in the weak-link regime for $d = 3$.

Strain at the Limit of Linearity (γ_o). The strain at the limit of linearity is the point at which the weakest bond in a floc breaks upon applying a force beyond a critical value. Above the limit of linearity, the network is broken and the linear elastic behavior does not exist anymore. According to the model of Shih et al.,[18] the relationship between the strain at the limit of linearity (γ_o) and solids' volume fraction for the strong link regime is

$$\gamma_o \sim \Phi^{[-(1+x)/(d-D)]} \tag{3}$$

From eq 3, we can deduce that the strain at the limit of linearity γ_o should decrease with increasing the solids' volume fraction Φ. In contrast, γ_o increases with increasing Φ for the weak-link regime ($d = 3$) as

$$\gamma_o \sim \Phi^{1/(d-D)} \tag{4}$$

A practical way to pinpoint whether a system is in the strong-link or weak-link regimes is by determining the dependence of the strain at the limit of linearity on the solids' volume fraction.

In our work, we determined the stress at the limit of linearity (σ_o) [Pa] that was then used instead of γ_o since $\sigma_o \sim \gamma_o$ in the linear viscoelastic region (LVR). Therefore, σ_o could be used as a function of Φ to determine the fractal dimension, assuming a weak-link regime using

$$\sigma_o \sim \Phi^{1/(d-D)} \tag{5}$$

Experimental Section

Samples. Samples of anhydrous milk fat (AMF), palm oil (PO), and cocoa butter (CB) were used in this study. Samples were melted at a high temperature (80 °C) for 30 min before dilution with canola oil to erase any crystal history. A higher temperature (120 °C) was used in PO because of its high maximum melting temperature. Different amounts of commercial-grade canola oil were mixed with fats to achieve different SFC values. More than eighty dilutions were prepared for each fat in 2% increments. Samples were stored in a refrigerator (2 °C).

Solid Fat Content (SFC). Samples were first melted at 80 °C for 30 min (120 °C for PO), to erase the crystal history, and mixed thoroughly to ensure homogeneity. Glass NMR tubes (10-mm diameter) were filled with approximately 3 g of sample and were then kept in a refrigerator at 5 °C for 24 h. SFC (%) measurements were then taken using pulsed nuclear magnetic resonance (pNMR) with a Bruker PC/20 series NMR Analyzer (Bruker, Milton, ON, Canada). Three tubes were prepared for each mixture and one measurement was carried out on each mixture. The average value of these three replicates was used in further analysis.

Rheology. Rheological measurements at small deformations were performed using a controlled stress AR2000 Shear Dynamic Rheometer (TA Instruments, Mississauga, ON, Canada). Sandpaper (Grade-60 for wood) was glued to the upper and lower 2-cm plates using Krazy Glue to prevent slippage. The sample platform temperature was controlled using a Peltier element, allowing samples to be analyzed at the specified temperature (i.e., 5 °C). Melted samples were poured into precooled cylindrical plastic molds of uniform diameter (20 mm) and thickness (3.2 mm) and were crystallized and stored at 5 °C for 24 h. Compression was set to a standardized normal force of 10 N for samples with an SFC greater than 30% and contact for samples with an SFC smaller than 30%. This ensures good contact between the parallel plate attachment and the fat sample. The linear viscoelastic region (LVR) for each sample was first determined by performing oscillatory stress sweeps from 0.65 to 1000 Pa for samples having low SFCs (less than 30%) and from 0.60 to 15000 for samples having high SFCs (more than 30%), at a constant frequency of 1 Hz. A total of 480 samples (80 dilutions × 6 replicates) were measured for each fat. The average value of these six replicates was used in further analysis.

Crystallization and Melting. The crystallization and melting behaviors of the three fats at different SFCs were studied by differential scanning calorimetry (DSC). Completely melted (120 °C for 30 min) and well-mixed fat samples (8−12 mg) were pipetted into aluminum pans and hermetically sealed. An empty

pan of known weight was used as the reference pan. Pans were then transferred to a Dupont Model 2910 DSC (TA Instruments, Mississauga, ON, Canada). Samples were heated to 80 °C and equilibrated for 30 min to erase crystal memory, and then cooled to 5 °C at 1 °C/min and kept for 10 min (crystallization). Samples were then heated to 80 °C at 5 °C/min (melting). Fresh samples of the three diluted fat systems were measured using the same temperature program. The onset of crystallization was estimated from the temperature value at which the exothermic peaks started to rise (i.e., deviate from the baseline), whereas melting temperatures were estimated from the endothermic peak maxima.

Polarized Light Microscopy (PLM). Fats were heated at 120 °C for 30 min to erase crystal memory. All glassware was preheated to 80 °C to avoid crystallization of the melted fats during sampling. A small droplet (~10 μL) of the melted fat was placed on a microscope glass slide (25 mm × 75 mm × 1 mm). A cover slip (22 mm × 22 mm) was then placed parallel to the plane of the slide and centered on the drop of sample to ensure that the sample thickness was uniform (~20 μm). The microscope slides and covers were purchased from Fisher Scientific (Fisher finest, Pittsburgh, PA). Four slides of each sample were stored at 5 °C in a refrigerator for 24 h or less depending on the experiment. Samples were then observed under polarized light using an Olympus BH polarized light microscope (Olympus, Tokyo, Japan). A Linkam LTS 350 large heating and freezing stage operated by a Linkam TP93 temperature programmer (Linkam Scientific instruments Ltd, Surrey, England) was used to maintain the temperature of the slides at 5 °C during imaging. A continuous flow of liquid nitrogen (BOC gases, Guelph, Ontario) was used to cool the stage. Images were acquired with a Sony XC-75 CCD video camera (Sony Corporation, Japan) with the gain switch in the auto position. The images were digitized using a Scion LG-2 PCI frame grabber board and using Scion Image software (Scion Corporation, Fredrick, MD). Image quality was enhanced by taking the average of 16 frames and by applying a background correction, using the Scion software. Three images were captured from each of four slides at the same time−temperature combination.

Image Processing and Fractal Dimension Determination. Images were processed using Adobe Photoshop 6.0 (Adobe Systems Inc., San Jose, CA). Original images (640 × 480 pixels) were first converted to 8 bit mode with their contrast adjusted to the level at which the actual microstructures, seen under polarized light, were all represented. Images were then inverted and thresholded using the bilevel autothreshold command.

The mass fractal dimension (D) was estimated by two image analysis methods: box-counting and particle-counting. The box-counting method requires that the features to be analyzed appear white and hence the images were not inverted before thresholding. The box-counting analysis was performed using Benoit 1.3 (Truesoft Int'l, St. Petersburg, Fl, www.trusoft-international.com). The slope of the log−log plot of the number of filled boxes versus the box side length corresponds to D_b. The D_b value was estimated using box side lengths in the range of 10−100 pixels. In the particle-counting method, the thresholded and inverted images were analyzed using a particle-counting algorithm in which the number of reflections, or particles, within boxes of decreasing size (5% increments), are counted. The slope of the log−log plot of the number of particles versus the box size is equal to D_f. The D_f was determined by averaging counts including and excluding particles that touch the perimeter of the region of interest (ROI) box.

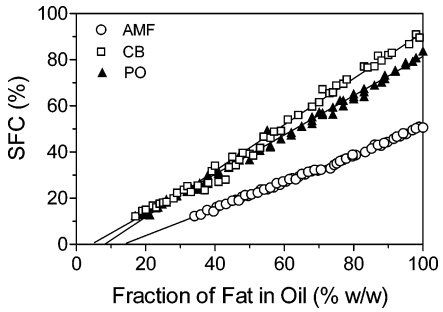

Figure 1. Relationship between the fraction of fat diluted in canola oil and solid fat content (SFC) for anhydrous milk fat (AMF), palm oil (PO), and cocoa butter (CB). The crystallization was performed at 5 °C for 24 h.

Thick Sample Preparation. About 4−5 drops of the heated and well-mixed melt were transferred into a metal ring (300 μm height) placed on a glass slide and was then covered with a cover slip. Care was taken to avoid tilting of the slide and the contact between the sample and the cover slip to allow the spatial distribution of microstructures in three dimensions without confinement effects. The sample was then kept in a refrigerator for 24 h at 5 °C, or directly monitored during crystallization inside the thermostatically controlled platform mentioned above. Images were acquired with a Retiga 1300 Cooled Mono 12-bit CCD video camera (Q-imaging, corporation, Burnaby, B. C., Canada) mounted on a motorized tube with two camera exits in a fully automated Leica DM RXA2 microscope (Leica Microsystems Wetzlar GmbH, Germany) equipped with a motorized focus drive that travels 25 mm at 0.015 μm increments. It also has a motorized and interchangeable X−Y stage z-control and additional control for separate z-movement. The Leica CTR MIC electronics box contains the external power unit for the lamp and the motorized microscope units as well as the electronic cards for driving the motorized functions on the microscope. Image enhancement and acquisition were performed using Openlab 3.1 software (Quorum Technologies Inc., Guelph, ON, Canada, www.improvision.com) run on a Machintosh G4 computer.

Pattern Analysis. Break points in graphs were determined both visually and by an iterative Pearson correlation coefficient maximization criterion. Linear regressions of putative linear regions within graphs were generated initially on the basis of visual assessment (initial conditions). Points were then added to the extremes of the initially chosen linear regions. Improvements, or no change, in the correlation coefficient lead to the incorporation of those points into that linear region. A greater than 5% decrease in the correlation coefficient because of inclusion of adjacent points lead to the exclusion of those points from the linear region. This is how the different linear regions were identified.

Results and Discussion

Figure 1 shows the SFC values as a function of dilution for the three fats. For all fats, increasing the amount of canola oil decreased the SFC in a linear fashion. In addition, the linear trend and the absolute SFC values were different between fats, mainly because of the large differences in composition. Worthy of notice is that the linear regression line for the different fats will not intercept the x-axis at a value of 0 (100% canola oil) when the SFC is zero. The x-intercepts for AMF, CB, and PO were 13.6, 8.2, and 4.3, respectively. This effect is probably due to the solubilization of a certain amount of the fats into the canola oil even under conditions of rapid cooling at high degrees

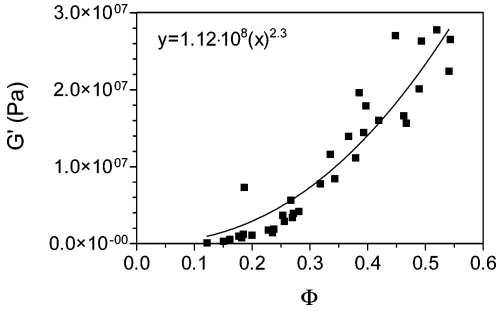

Figure 2. Power−law relationship between the storage modulus (G') and the solids' volume fraction (Φ = SFC/100) for cocoa butter in the SFC range [12, 40%].

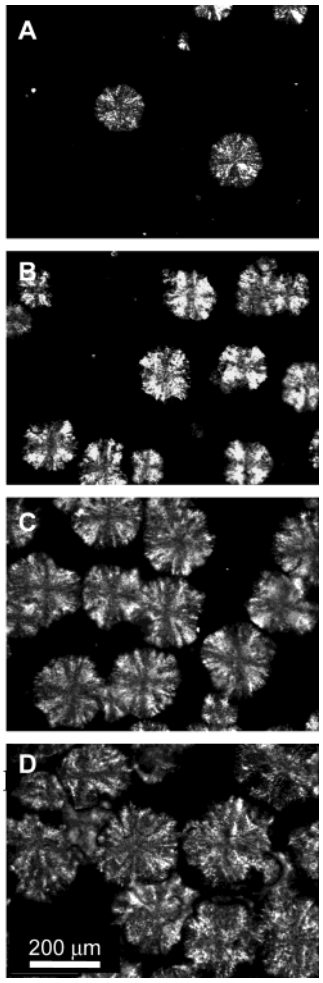

Figure 3. Polarized light micrographs of CB thick samples (20% SFC) crystallized at 5 °C for (A) 1 h, (B) 3 h, (C) 8 h, and (D) 20 h.

of undercooling. This is an important point, since the rheological technique for fractal dimension determination requires that the solvent used (i.e., the canola oil at 5 °C in our case) only dilute, and not dissolve, solid network material. This solubilization could have an effect on the rheological determination of the fractal dimension of a fat crystal network, and constitutes a limitation of this method. This effect is, however, system-dependent.

Fat Crystal Network as a Particle Gel? Figure 2 shows plots of the shear storage modulus (G') veresus SFC for AMF. The relationship of G' to SFC is a nonlinear, power law type relationship, as for a colloidal gel. This power−law relationship can be exploited to obtain structural information of the fat crystal networks, such as the spatial distribution of mass (mass fractal

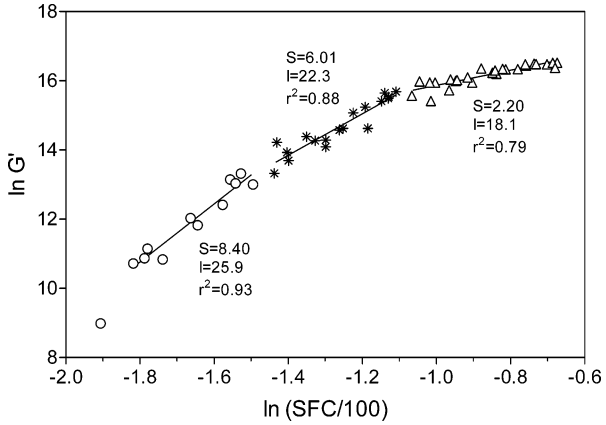

Figure 4. Relationship between the storage modulus (G') of and the solids' volume fraction (Φ = SFC/100) for anhydrous milk fat. S = slope, I = y-intercept, r^2 = Pearson correlation coefficient of the linear regression lines.

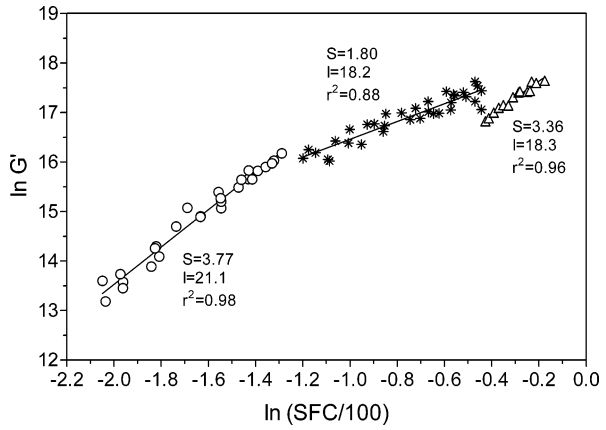

Figure 5. Relationship between the storage modulus (G') of and the solids' volume fraction (Φ = SFC/100) for palm oil. S = slope, I = y-intercept, r^2 = Pearson correlation coefficient of the linear regression lines.

dimension). Moreover, Figure 3 shows the fat crystal network in cocoa butter as clusters of crystallites, quite similar in nature to fractal colloidal aggregates described in the literature.[17−22] These samples were allowed to crystallize freely on a glass slide without a coverslip so that the structure of the fat crystal network could be observed without confinement effects. The micrographs show that CB formed clusters of crystallites, which increased in size and number as a function of time, to the point where the clusters touch their nearest neighbors. Further deposition of solids will only coarsen the network without affecting cluster size. Our observations suggested that upon crystallization, these fats formed a network of polycrystalline crystal clusters, similar in nature to colloidal gels.

Rheology. To estimate the mass fractal dimension (D) of fat crystal networks, it was necessary to determine the storage modulus at varying SFCs. Small deformation rheological tests were performed to obtain the shear storage modulus (G') of the blends in the linear viscoelastic region (LVR). The log−log plot of G' versus Φ (SFC/100) yielded a straight line with slope (μ). This slope was used to estimate D. This mass fractal dimension is for an object embedded in three-dimensional Euclidean space. The rheological results of AMF, PO, and CB at different SFC values are shown in Figures 4, 5, and 6, respectively. AMF and PO displayed three different linear regions, yet only two regions were identified in CB. These regions indicated different mechanical responses in the same material depending on the solids' concentration. The existence

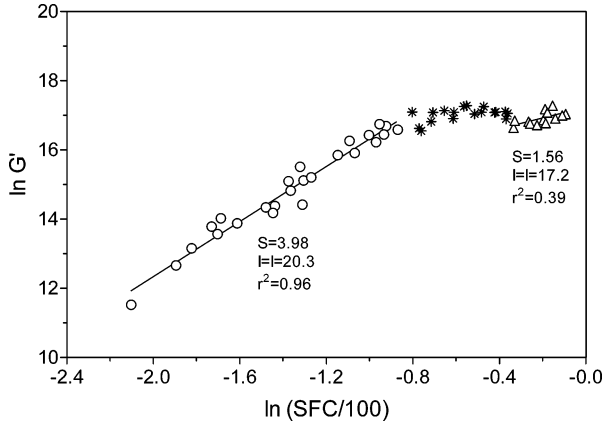

Figure 6. Relationship between the storage modulus (G') of and the solids' volume fraction (Φ = SFC/100) for cocoa butter. S = slope, I = y-intercept, r^2 = Pearson correlation coefficient of the linear regression lines.

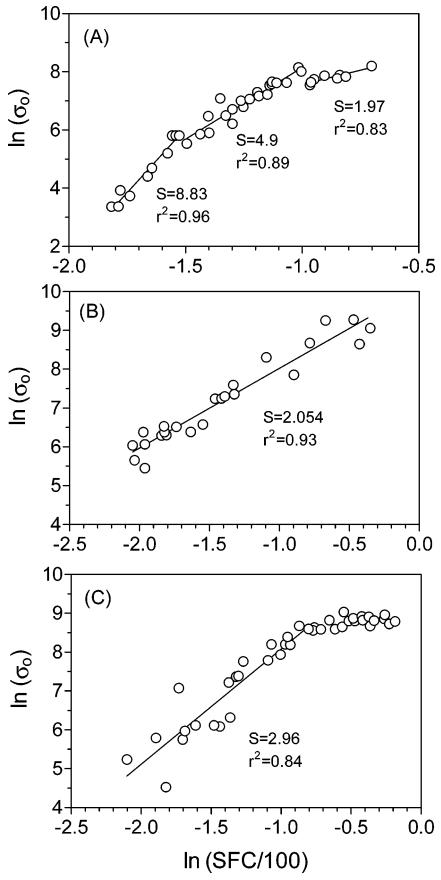

Figure 7. Relationship between the stress at the limit of linearity (σ_o) and the solids' volume fraction (Φ = SFC/100) for blends of (A) anhydrous milk fat, (B) palm oil, and (C) cocoa butter.

of these regions could be interpreted as the fat crystal network in the weak, intermediate, and strong-link regimes, in order of decreasing SFC. To test the above hypothesis, the dependence of the stress at the limit of linearity on Φ was studied. The stress at the limit of linearity (σ_o) was estimated from plots of the storage modulus (G') to the applied oscillatory stress. σ_o was estimated as the stress at which the storage modulus (G'), as well as the loss modulus (G''), started to deviate from a constant value. The σ_o determined in our studies always increased with increases in Φ for the three fats (Figure 7). This suggested that the three fat systems were in the weak-link regime in the entire SFC range studied. Accordingly, the fractal dimensions assuming the weak-link regime were calculated for each fat, as shown in Table 1. The values obtained assuming the weak-link regime were quite reasonable and comparable to previously reported values in our laboratory.[10] In contrast, calculation of D assuming a strong-link behavior yielded unreasonable estimates (Table 1).

TABLE 1: Fractal Dimension (D) for Anhydrous Milk Fat (AMF), Palm Oil (PO), and Cocoa Butter (CB) at Low, Intermediate, and High Solid Fat Contents (SFC) Determined from Rheological Measurements

	SFC (%)	D_{WLR} [a]	D_{SLR} [b]	$D\sigma_o$ [c]
AMF	37−51	2.54	1.18	2.49
	21−35	2.83	2.33	2.79
	12−20	2.88	2.52	2.89
PO	64−78	2.70	1.81	
	31−59	2.44	0.77	2.51
	16−26	2.73	1.94	2.51
CB	72−90	2.36	0.43	
	12−47	2.75	1.99	2.66

[a] D_{WLR}, fractal dimension determined assuming the weak-link regime. [b] D_{SLR}, fractal dimension determined assuming the strong link regime. [c] $D\sigma_o$, fractal dimension determined from the stress at the limit of linearity.

Determinations of the stress at the limit of linearity indicated that all fats were in the weak-link regime. Shih et al.[18] defined the strong-link regime at particle concentrations below 10%, where the strain at the limit of linearity (γ_o) increased as a function of Φ. In our study, rheological tests were difficult to perform at these low SFC levels because the fats became too soft to be analyzed. The lowest SFC that could be studied was 12%.

Scaling Behavior of σ_o with SFC. Figure 7 shows changes in σ_o as a function of Φ for blends of milk fat (Figure 7a), palm oil (Figure 7b), and cocoa butter (Figure 7c). The fractal dimensions of the three fat crystal networks were determined from the slope of the log−log plot of σ_o versus Φ, assuming a weak-link rheological regime [$D = 3$-(slope)$^{-1}$], and are reported in Table 1. The fractal dimensions calculated using the storage modulus (i.e., G' vs Φ) and the stress at the limit of linearity (i.e., σ_o vs Φ) were comparable (Table 1). Three different regions were identified for AMF (Figure 7a) and two regions in CB (Figure 7c), in agreement with the $G'-\Phi$ results. For PO, however, no breaks in the log−log plot were observed. This points to system-specific effects on G' and σ_o.

Crystallization and Melting Behavior. Figure 8 shows plots of the onset of crystallization (T_c) as a function of SFC for AMF, PO, and CB. Increasing the canola oil mass fraction, or decreasing the SFC, caused a gradual decrease in T_c as expected from colligative property arguments (freezing point depression). For example, the T_c of AMF at high SFC (52%) decreased from 17.5 °C to 16.0 °C (35% SFC) and to 9.0 °C (16% SFC), as shown in Figure 8A. As can be appreciated, the crystallization behavior of PO (Figure 8B) and CB (Figure 8C) were also similar. The break points, identified by arrows in Figure 8, as well as the span of the linear regions were very similar (not identical) to those identified in G' versus SFC plots. This indicated a possible relationship between the mechanical properties of the material and the kinetics of crystallization.

Peak melting temperatures also decreased with decreasing SFC for the three fats (Figure 9). Using these data, the solubility of fat crystals in canola oil was studied using the Hildebrand model:[27,28]

$$\log_{10} x = \frac{\Delta H}{R}\left(\frac{1}{T_m^{HMF}} - \frac{1}{T_m}\right) \quad (6)$$

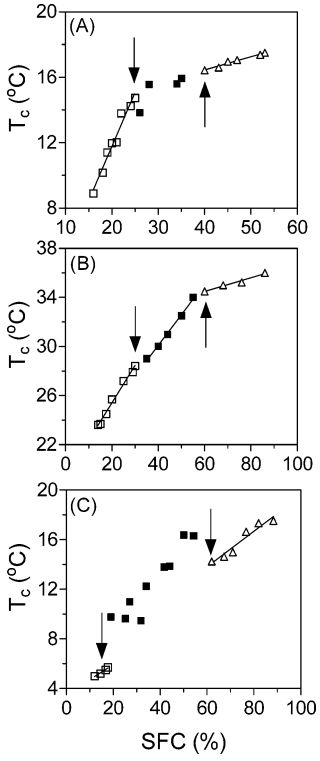

Figure 8. Changes in the crystallization onset temperature (T_c) as a function of solid fat content (SFC) for (A) AMF, (B) PO, and (C) CB. The arrows indicate the break points.

where x is the mole fraction of solid fat (x = SFC/100 in our case) and T_m is the peak melting temperature of the mixture and T_m^{HMF} corresponds to the melting temperature of the highest-melting fraction (HMF) in the mixture. A straight line in a log x versus $1/T_m$ plot is suggestive of ideal solubility of the fat crystals in canola oil. Figure 9D−F shows plots of log x versus $1/T_m$ for AMF, PO, and CB, respectively. Three linear regions were identified for AMF (Figure 9D) and PO (Figure 9E), whereas only two regions were identified for CB (Figure 9F). This was in agreement with the patterns observed in the T_c−SFC plots (Figure 8). The heats of fusion (ΔH) determined from the slopes increase as a function of increasing dilution. ΔH increased from 31.2, 64.8, and 38.7 kJ/mol to 51.8, 158, and 66.3 kJ/mol for AMF, PO, and CB, respectively. The increase in ΔH as a function of increasing dilution is indicative of the formation of less mixed (more pure or homogeneous) crystals. The formation of more pure crystals at higher dilutions is mainly due to decreases in diffusional limitations (because of a lower melt viscosity), as well as decreases in the rates of nucleation and growth (because of decreases in the supersaturation of the melt). These two factors—greater molecular mobility and a slower crystallization process—allow for the formation of more pure crystals at higher dilutions. The different linear regions observed in Figure 9 are indicative of the formation of different polymorphic forms, different solid solutions,[29] imperfect crystals,[30] or combinations[31] thereof, depending on the concentration of crystallizing material.

On the basis of the above results, we postulate that different crystal types (polymorphs or solid phases) are formed depending on solids' content. These changes in solution behavior were probably responsible for the changes observed in the crystallization behavior of the material, which eventually translated into different mechanical properties. It would stand to reason, therefore, that the microstructure of the material would also be

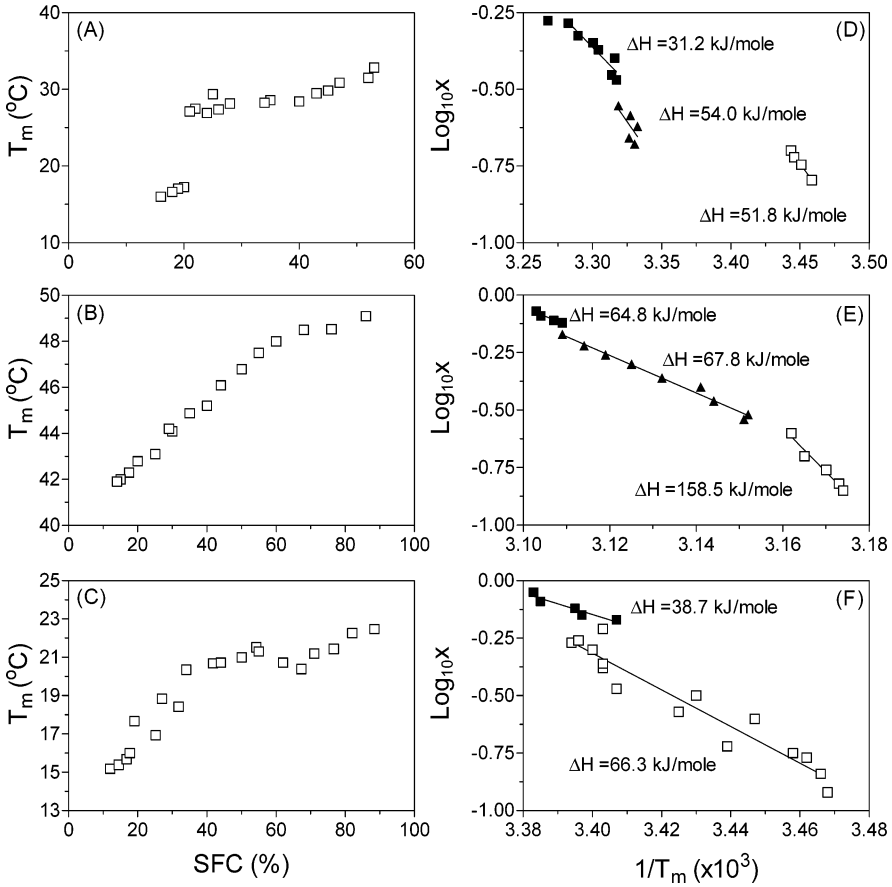

Figure 9. Changes in the peak melting temperature (T_m) as a function of SFC for (A) AMF, (B) PO, and (C) CB, and Hildebrand plots for (D) AMF, (E) PO, and (F) CB.

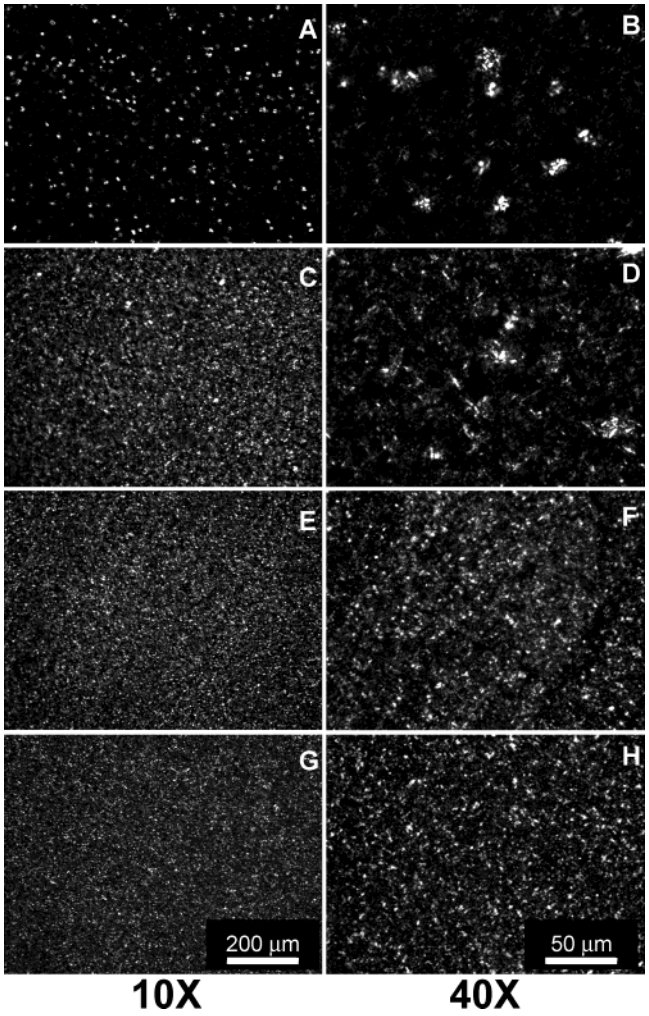

Figure 10. Polarized light micrographs of AMF crystallized in 20 μm films at 5 °C for 24 h. The SFC values are (A, B) 12%, (C, D) 19%, (E, F) 35%, and (G, H) 51%.

affected by changes in solution behavior and crystallization kinetics.

Polarized Light Microscopy. The microstructure of the fats was observed by polarized light microscopy. Figure 10 shows polarized light micrographs of AMF taken at different magnifications. As can be appreciated, relatively large clusters were observed at 12% SFC (Figure 10A, B) and by increasing the SFC to 19%, the clusters decreased in size and increased in number (Figure 10C, D). The SFC of the samples in Figure 10A−D corresponds to the low SFC region (12−20%). In the intermediate SFC (21−35%) and high SFC ranges (above 37%), only small crystallites were evident (Figure 10E−H). Figure 11 shows micrographs of the PO samples. Large clusters were observed in the low SFC range (16−26%) (Figure 11A, B), while combinations of small and a few large clusters were observed in the intermediate SFC region (31−59%) (Figure 11C, D). In the highest SFC range (64−78%), samples showed combinations of large clusters and smaller crystallites filling the spaces between clusters (Figure 11E, F). Although the large clusters grown at low SFCs (Figure 11A, B) were similar in morphology to those at higher SFCs (Figure 11C−F), small crystallites were not observed at low SFCs.

For CB at low SFCs (19%), large and irregular-shaped spherulites were observed (Figure 12A). By increasing the SFC to 25%, spherulites increased in size, maintaining the same shape (Figure 12B). Between 34 and 42% SFC, however, spherulites

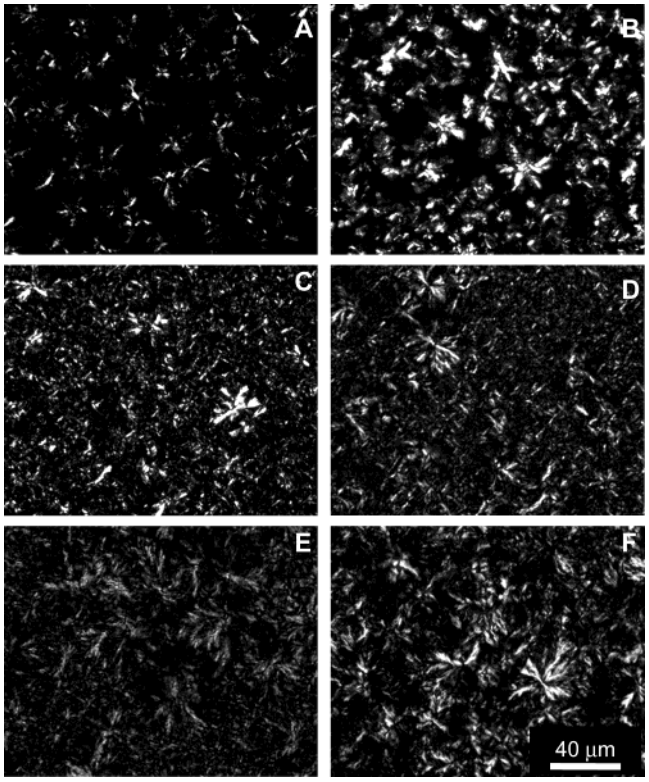

Figure 11. Polarized light micrographs of PO crystallized in 20 μm films at 5 °C for 24 h. The SFC values are (A) 16%, (B) 17.5%, (C) 42.5%, (D) 55%, (E) 70%, and (F) 75%.

were much more regular (Figure 12C, D). By increasing the SFC to 54%, the clusters became more spherical and displayed a fine, granular texture (Figure 12E), quite different from the spherulites observed at low SFCs (Figure 12A−D). Above 54%, only a fine mass of crystallites was observed (Figure 12F−H).

The effects of varying SFC on cluster size were also monitored in freely crystallized (nonconfined) CB samples at low and high SFCs. At low SFC (20%), a few large clusters (200 μm) were observed (Figure 13A) while more numerous small clusters (50−60 μm) were observed at high SFC values (70%), as shown in Figure 13B.

In general, at higher dilutions (lower SFCs), larger clusters were observed. This effect is in agreement with the observed increases in the fractal dimension of the fat crystal networks at lower SFCs (Table 1). Fractal cluster size (ξ) scales with the solids' volume fraction (Φ) as

$$\xi \sim \Phi^{1/(D-d)} \tag{7}$$

where D is the mass fractal dimension and d is the Euclidean dimensionality of the embedding space. Thus, a decrease in SFC and an increase in the fractal dimension would lead to an increase in cluster size. The change in cluster size occurs in a narrow range of SFCs, thus pointing to the fractal dimension as being an important factor in determining cluster size. In the weak link regime, the fractal dimension simply defines the cluster size, and cluster size is the only factor influencing the mechanical response of the material, since the cluster itself does not deform.

Image Analysis. Figure 14 shows changes in the box-counting fractal dimension (D_b) for the spatial distribution of mass within the fat crystal networks as a function of SFC using images acquired at low (10× objective) and high magnifications (40× objective). The overall results indicated that D_b increased

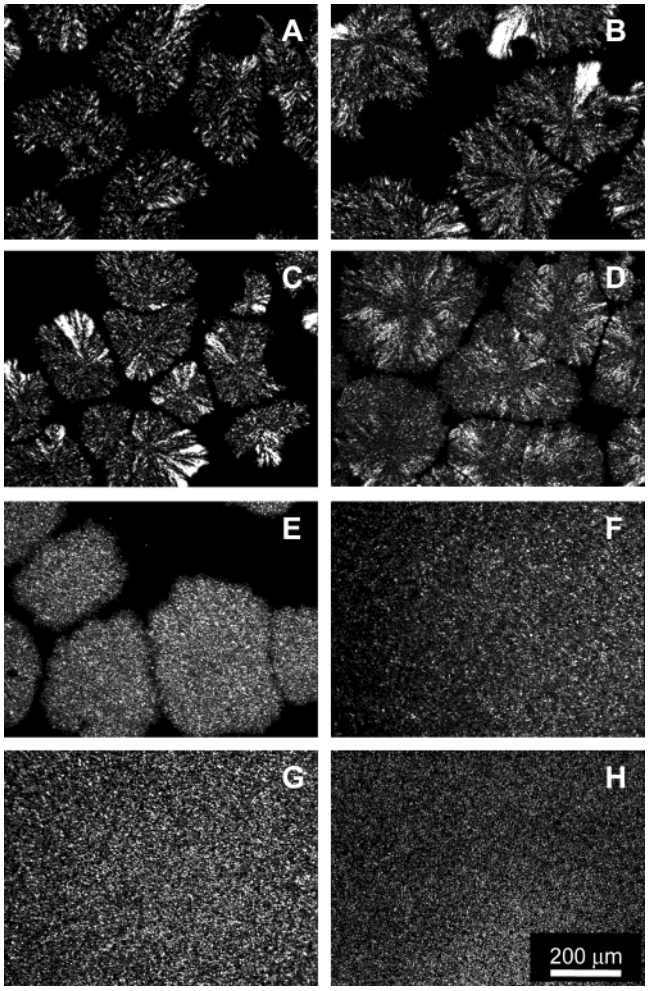

Figure 12. Polarized light micrographs of CB crystallized in 20 μm films at 5 °C for 24 h. The SFC values are (A) 19%, (B) 25%, (C) 34%, (D) 42%, (E) 54%, (F) 60%, (G) 65%, and (H) 85%.

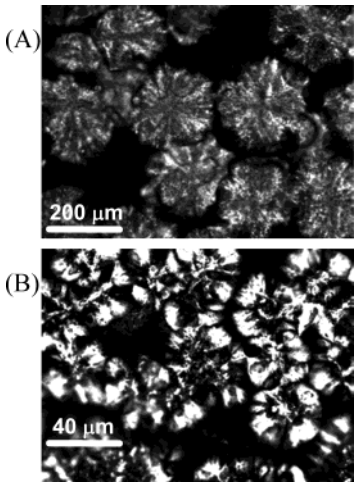

Figure 13. Polarized light micrographs of CB thick samples (A) low SFC (20%) and (B) high SFC (70%).

with increasing SFC, reaching a plateau at high SFC values. Analysis of the images of AMF taken at both magnifications (Figure 14A) indicated no significant increase in D_b with increasing SFC from the intermediate SFC region (21−35%) to the high SFC region of (37−51%). In addition, the SFC value at which the D_b became constant was similar to the break point at 22% SFC observed in the T_c−SFC curve (Figure 8A). Similar behavior was also shown for PO (Figure 14B), with a break

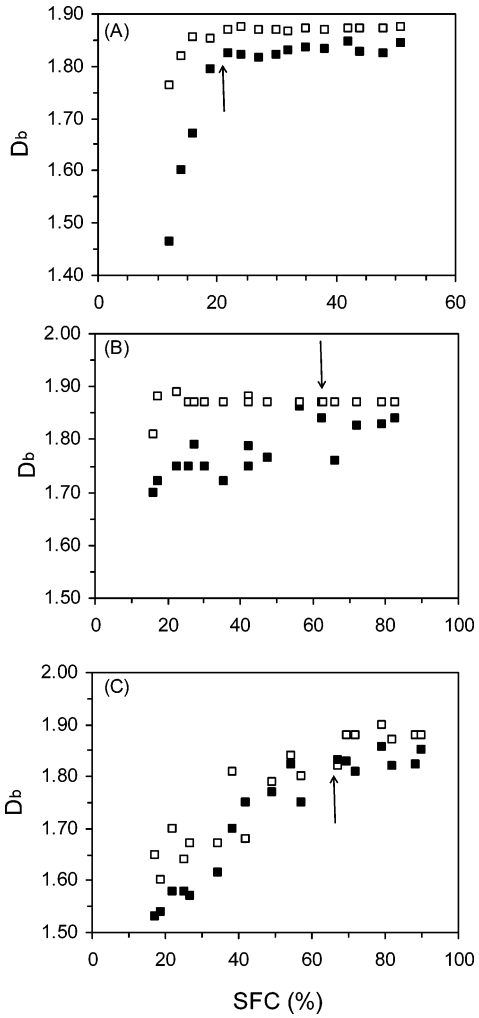

Figure 14. Changes in the box-counting fractal dimension (D_b) as a function of SFC for (A) AMF, (B) PO, and (C) CB. The arrows indicate the break points. The open squares indicate the analysis of images acquired using the 10× objective, while the closed squares indicate the analysis of images acquired using the 40× objective.

point occurring at 62% SFC similar to the high SFC break point shown in Figure 8B. In CB (Figure 14C), D_b increased gradually as a function of SFC similarly at both magnifications. Above 67% SFC, the curve became flat, in agreement with the high SFC break point shown in Figure 8C. These results agreed well with the CB images (Figure 12), which showed diversity in microstructures at different SFC. Accordingly, the lower D_b values corresponded to larger microstructures at low SFC, whereas samples having a large number of smaller clusters at higher SFC were characterized by higher D_b. Fractal dimensions did not vary above a critical SFC because fat crystals filled space homogeneously on the microscope slide. Nevertheless, the similarity between the break points in Figure 14 (D_b) and those in Figure 8 (T_c) indicates sensitivity of the box-counting fractal dimension to changes in crystallization kinetics and polymorphism. Previous work from our group[32,33] has shown that D_b is strongly correlated to crystallization kinetics and polymorphism in CB and in mixture of milkfat fractions and CB.

In the particle-counting method, D_f increased as a function of SFC for PO, yet no clear trends were observed for AMF and CB and, thus, an average D_f value was determined for AMF (1.93 ± 0.02) and CB (1.90 ± 0.08). This points to a limitation of this method when the material in question fills space homogeneously and fully, particularly at high solids' contents.

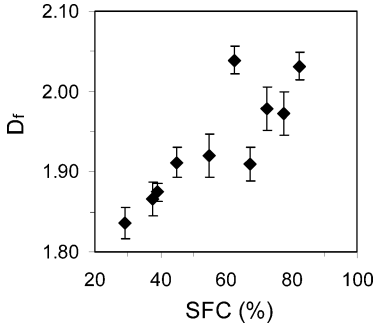

Figure 15. Changes in the fractal dimension determined by the particle-counting method (D_f) as a function of SFC for PO.

Figure 15 shows the plot of SFC versus D_f for PO. As can be appreciated from the figure, a significant linear trend extended up to 45% SFC and then there is a plateau after which D_f increased again.

The usefulness of the fractal dimension in explaining differences in elasticity between fats can be easily demonstrated. Work from our group[14] has shown that the elastic modulus of a fat is related to the solids' content (Φ) and the structure of its fat crystal network by

$$G' = \lambda\Phi^{\mu} \tag{8}$$

where λ and μ are constants related to structural characteristics of the network. The usefulness of this model becomes obvious when trying to model changes in mechanical properties between fats at the same SFC. For example, the G' at an SFC of 27.2% ($\ln(\mathrm{SFC}/100) = -1.3$) differs between fats (Figures 4−6). The $\ln G'$ for AMF, PO, and CB are, respectively, 14.4, 16.2, and 15.3, while the rheologically determined fractal dimensions are 2.83, 2.73, and 2.75, respectively (Table 1). Thus, a decrease in the fractal dimension of a system, at equal SFC, leads to an increase in the G' of the system. Changes in the G' across systems can be quantified by

$$\ln G'_1 - \ln G'_2 = \ln \lambda_1 - \ln \lambda_2 + (\mu_1 - \mu_2)\ln(SFC/100) \tag{9}$$

A quick calculation using the parameters listed in Figures 4−6 ($\mu = S$ and $\ln \lambda = I$) will quickly demonstrate how changes in G' can be explained in part by changes in the fractal dimension of the fat crystal network. Certainly, changes in crystallite size and morphology will also strongly influence mechanical properties.

We have shown that changing blend composition, or the SFC of three fats, affected the mechanical properties in terms of the elastic modulus and the stress at the limit of linearity, and this change is due to, in part, changes in the fractal dimension of the network. Although fats showed different mechanical responses as a function of SFC, they all were in the weak-link rheological regime. The relationship between SFC and either the G' or σ_o offered two ways of determining the mass fractal dimension of a fat crystal network. These results lend strong support to the application of fractal scaling theories to colloidal networks of fat crystals. Network structure was highly affected by varying the SFC, which was accompanied by alterations in solution behavior and crystallization kinetics of the material. Therefore, changes in microstructure, induced by changes in crystal-melt solution behavior and crystallization kinetics, resulted in different mechanical properties of the fats.

As a final remark on the results of the current work, consideration of the different levels of structures starting from the early stages of crystallization (nanometer/molecular scale) to macromolecular network formation (micrometer/mesoscale) provides considerable information, which may help link fat crystal network microstructure to mechanical properties. Crystallization conditions and chemical composition can be then manipulated to control final network structure and consequently the macroscopic rheological properties of fats.

Acknowledgment. The authors acknowledge the financial assistance of the Natural Sciences and Engineering Research Council of Canada (NSERC) and the Ontario Ministry of Agriculture and Food (OMAF).

Note Added after ASAP Posting. This article was posted ASAP on 11/27/2003. A change has been made in the first paragraph of the Results and Discussion section. The correct version was posted on 12/03/2003.

References and Notes

(1) Heertje, I. *Food Structure* **1993**, *12*, 77−94.
(2) Juriaanse, A. C.; Heertje, I. *Food Microstructure* **1988**, *7*, 181−188.
(3) Narine, S. S.; Marangoni, A. G. *Food Res. Intl.* **1999**, *32*, 227−248.
(4) Wright, A.; Scanlon, M. G.; Hartel, R. W.; Marangoni, A. G. *J. Food Sci.* **2001**, *66*, 1056−1071.
(5) Marangoni, A. G. *Trends Food Sci.Technol.* **2002**, *13*, 37−47.
(6) Van den Tempel, M. *J. Colloid Interface Sci.* **1961**, *16*, 284−296.
(7) Van den Tempel, M. *J. Colloid Interface Sci.* **1979**, *71*, 18−20.
(8) Vreeker, R.; Hoekstra, L. L.; den Boer, D. C.; Agterof, W. G. M. *Colloids Surf.* **1992**, *65*, 185−189
(9) Marangoni, A. G.; Rousseau, D. *J. Am. Oil Chem. Soc.* **1996**, *73*, 991−994.
(10) Narine, S. S.; Marangoni, A. G. *Phys. Rev. E* **1999**, *59*, 1908−1920.
(11) Awad, T. S.; Pelan E.; Marangoni, A. G. Margarine: an example of a particle gel. In *Soft Food Materials: Functionality of structures*; Marcel Dekker (In press).
(12) Marangoni, A. G. *Phys. Rev. B* **2000**, *62*, 13951−13955.
(13) Narine, S. S.; Marangoni, A. G. *Phys. Rev. E* **1999**, *60*, 6991−7000.
(14) Marangoni, A. G.; Rogers, M. A. *Appl. Phys. Lett.* **2003**, *82*, 3239−3241.
(15) Kantor, Y.; Webman, I. *Phys. Rev. Lett.* **1984**, *52*, 1891−1894.
(16) Brown, W. D. Doctoral Thesis, University of Cambridge, 1987.
(17) Bremer, L. G. B.; van Vliet, T.; Walstra, P. *J. Chem. Soc., Faraday Trans.* **1989**, *185*, 3359−3372.
(18) Shih, W. H.; Shih, W. Y.; Kim, S. I.; Liu, J.; Aksay, I. A. *Phys. Rev. A* **1990**, *42*, 4772−4779.
(19) Sonntag, R. C.; Russel, W. B. *J. Colloid Interface Sci.* **1987**, *116*, 485−489.
(20) Buscall, R.; Mills, P. D. A.; Goodwin, J. W.; Lawson, D. W. *J. Chem. Soc., Faraday Trans.* **1988**, *84*, 4249−4260.
(21) Hagiwara, T.; Kumagai, H.; Masunaga, T.; Nakamura, K. *Biosci. Biotechnol. Biochem.* **1997**, *61*, 11663−1667.
(22) Wu, H.; Morbidelli, M. *Langmuir* **2001**, *17*, 1030−1036.
(23) Wright, A. J.; Marangoni, A. G. *J. Food Sci.* **2003**, *68*, 182−186.
(24) Marangoni, A. G.; McGauley, S. E. *Cryst. Growth Design* **2002**, *35*, 95−108.
(25) Marangoni, A. G.; Narine, S. S. *Food Res. Intl.* **2002**, *35*, 957−969.
(26) Litwinenko, J. W.; Rojas, A. M.; Greschenson L. N.; Marangoni, A. G. *J. Am. Oil Chem. Soc.* **2002**, *79*, 647−654.
(27) Hildebrand, J. H.; Scott, R. L. In *Regular solutions*; Prentice Hall: Englewood Cliffs, 1962; pp 1−40.
(28) Timms, R. E. *Aust. J. Dairy Sci.* **1978**, *33*, 130−135.
(29) Mulder, H. *Neth. Milk Dairy J.* **1953**, 7, 149−174.
(30) Sherbon, J. W.; Coulter, S. T. *J. Dairy Sci.* **1966**, *49*, 1126−1131.
(31) Knoester, M.; de Bruijne, P.; van den Tempel, M. *Chem. Phys. Lipids* **1972**, *9*, 309−319.
(32) Marangoni, A. G.; McGauley, S. E. *Cryst. Growth Design* **2003**, *3*, 95−108.
(33) Marangoni, A. G.; Narine, S. S. *Food Res. Intl.* **2002**, *35*, 957−969.